Strain Effects on Oxygen Migration in Perovskites

Updated January 26, 2016. See Update Note.

Tam Mayeshiba

Materials Science Program

University of Wisconsin-Madison, Madison, WI, 53706, USA

Dane Morgan (Corresponding Author)

Department of Materials Science and Engineering,

University of Wisconsin-Madison, Madison, WI, 53706, USA

ddmorgan@wisc.edu

Update Note, January 26, 2016:
This draft was updated from the original version in order to:

1. Incorporate proof corrections that were made to the PCCP proof after submission, and which are not included in the previous Word document.
2. Correct the following error: The exponents of the Birch-Murnaghan equation in our Python-language equation of state code were erroneously given as 7/3, 5/3, and 2/3, which evaluated to 2, 1, and 0, respectively, instead of being given as 7.0/3.0, 5.0/3.0, and 2.0/3.0, evaluating to 2.333…, 1.666…, and 0.666…. These erroneously small exponents were applied to the ratio V_0/V which was less than 1, producing $P(V_0$, fixed V) that was steeper than it should have been. Therefore, every pressure difference $P_{saddle}(V_{0,saddle}$, fixed V) – $P_{initial}(V_{0,initial}$, fixed V) between a saddle point and initial point was reproduced at smaller intervals of V_0, or smaller fitted migration volumes, than was correct. Since the elastic strain model DMEPS scales linearly with migration volume (see Eq. 2 in the original paper), the resulting elastic strain model DMEPS were all smaller in magnitude than they should have been.
3. Correct minor data errors detected when the data was reorganized.

A short correction (1 page, with Figure 5R to correct Figure 5) was sent to PCCP in January 2016.

This updated version of the main paper and the updated version of the supporting information have not been peer-reviewed.

Abstract

Fast oxygen transport materials are necessary for a range of technologies, including efficient and cost-effective solid oxide fuel cells, gas separation membranes, oxygen sensors, chemical looping devices, and memristors. Strain is often proposed as a method to enhance the performance of oxygen transport materials, but the magnitude of its effect and its underlying mechanisms are not well-understood, particularly in the widely-used perovskite-structured oxygen conductors.

This work reports on an *ab-initio* prediction of strain effects on migration energetics for nine perovskite systems of the form $LaBO_3$, where B = [Sc, Ti, V, Cr, Mn, Fe, Co, Ni, Ga]. Biaxial strain, as might be easily produced in epitaxial systems, is predicted to lead to approximately linear changes in migration energy. We find that tensile biaxial strain reduces the oxygen vacancy migration barrier across the systems studied by an average of 65 meV per percent strain for a single selected hop, with a low of 36 and a high of 86 meV decrease in migration barrier per percent strain across all systems. The estimated range for the change in migration barrier within each system is +/- 25 meV per percent strain when considering all hops. These results suggest that strain can significantly impact transport in these materials, e.g., a 2% tensile strain can increase the diffusion coefficient by about three orders of magnitude at 300 K (one order of magnitude at 500°C or 773 K) for one of the most strain-responsive materials calculated here ($LaCrO_3$).

We show that a simple elasticity model, which assumes only dilative or compressive strain in a cubic environment and a fixed migration volume, can qualitatively but not quantitatively model the strain dependence of the migration energy, suggesting that factors not captured by continuum elasticity play a significant role in the strain response.

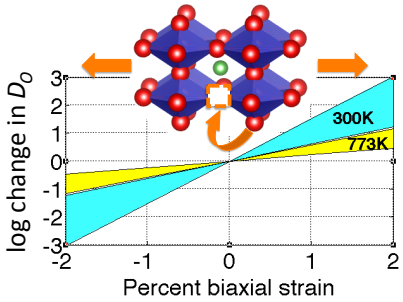

Computational results show that a 2% biaxial tensile strain may increase oxygen ion conduction, both in- and out-of-plane, by up to approximately three orders of magnitude at 300K in the most strain-sensitive $LaBO_3$ perovskites, where B = [Sc, Ti, V, Cr, Mn, Fe, Co, Ni, Ga].

Introduction

Fast oxygen transport materials are important for creating efficient and cost-effective solid oxide fuel cells (SOFCs), gas separation membranes, oxygen sensors, chemical looping devices, and memristors.[1-8] Besides changing the chemical makeup of a material or changing the operating conditions of the device (e.g., temperature), strain is another possible mechanism to enhance oxygen diffusion. In a broad review over both metals and oxides, Yildiz summarized that stress resulting from tensile strain on materials affects the energy landscape, particularly by weakening interatomic bond strengths, which then results in lower defect formation energy, dissociation barrier, charge transfer barrier, adsorption energy, and, of particular interest to this paper, oxygen migration barrier.[8]

Several experimental studies have shown that strain in oxygen-conducting oxides can lead to faster oxygen bulk or surface diffusion.[9-13] The strongest effect is cited for Yttria-stabilized ZrO_2 (YSZ) and $SrTiO_3$ (STO) interfaces at 8 orders of magnitude enhancement in ionic conductivity in a range around 100°C to 225°C. This effect was attributed to strain and interfacial disorder in the YSZ/STO interface.[9] However, combined experimental and computational studies of (YSZ or ceria, CeO_2)/STO interfaces now suggest elastic strain contributions of 2-4 orders of magnitude, and attribute the remaining orders of magnitude primarily to electronic conductivity, if they attribute them at all.[12-14]

A number of computational studies have also examined the effects of strain on oxygen migration, with most studies focusing on fluorite structures. To aid in this discussion, we introduce the term "DMEPS" for "Delta in (oxygen) Migration (barrier) Energy per Percent Strain," where a DMEPS value is the slope of a plot of migration barrier energy versus percent strain. DeSouza, Ramadan, and Hörner find a total of 0.5 eV (out-of-plane) to 0.6 eV (in-plane)

reduction in migration barrier for the fluorite CeO_2 at 7% biaxial tensile strain, with a migration barrier vs. strain slope of about -100 meV (out-of-plane) to -50 meV (in-plane) change per percent (biaxial) strain (i.e., DMEPS values of -100 meV/% strain and -50 meV/% strain, respectively) for low strains.[14] Note that in-plane refers to hop vectors entirely in the plane of the biaxial strain and out-of-plane refers to hop vectors with a component normal to the plane of biaxial strain. These studies were done using classical fitted pair potentials and correspond to about four orders of magnitude in ionic conductivity enhancement for 4% biaxial tensile strain at 500 K.[14] Schichtel, Korte, Hesse, and Janek predict a maximum of 2.5 orders of magnitude in ionic conductivity enhancement (only in-plane calculated) for a YSZ/STO lattice mismatch of 7.37% at 573 K using elastic strain theory.[12] With each 100 meV decrease in migration barrier producing a 0.88 increase in magnitude of conductivity at 573K (see Supporting Information Section S9), this value corresponds to a DMEPS of -38 meV/% strain. Kushima and Yildiz predict a maximum enhancement of 3.8 orders of magnitude (in-plane) for 4% biaxial tensile strain in YSZ at 400K using density functional theory migration barrier inputs into a kinetic Monte Carlo simulation.[15] Although their change of migration energy with strain is not linear, if it were, then this effect would correspond to a DMEPS of -75 meV/% strain. A density-functional theory study by Yang, Cao, Ma, Zhou, Jiang, and Zhong find a DMEPS of -50 to -90 meV/% strain for a single hop (out-of-plane, backwards and forwards; the slope is calculated between -1% and +1% strain) in the $A^{2+}B^{4+}O_3$ perovskite $BaTiO_3$, although interestingly their aim is to find a way to decrease oxygen migration in order to preserve ferroelectric behavior, and they propose compressive strain as a mechanism for doing so.[16] This last study underscores the point that, while the focus of this paper is on increasing oxygen migration, its findings could also apply to decreasing oxygen migration, for example for reducing corrosion.[8]

A number of explanations have been offered for the source of the coupling of migration energies and strain. Similar to the idea that doping with different-sized cations introduces local stress fields and lattice expansion, leading to lower migration energies,[8, 17] Kushima and Yildiz identified the mechanisms of strain effects on migration energies as a competition between the "elastic stretching" of cation-oxygen bonds, which weakens those bonds and also creates a larger "migration space," thus decreasing migration barrier, versus the plastic deformation of the material as bonds are completely broken and new, strong bonds are formed, thus increasing migration barrier.[15] Chroneos, Yildiz, Tarancón, Parfitt, and Kilner stress what they term "mechano-chemical" coupling as a mechanism, in which lattice strain affects the cation-oxygen bond strength.[18] Schichtel et al.'s elastic strain model, which has been used to predict changes in migration barrier with strain in YSZ and CSZ (Yttrium- and Calcium-stabilized zirconia) on various substrates, includes the isotropic pressure effects of strain, but neglects the changing local bond strengths mentioned by Chroneos et al.[12] While these studies to date shed some light on strain effects, there are still many uncertainties, and almost all studies have focused on the fluorite structure, leaving the important class of perovskite oxide oxygen conductors largely unexplored.

As a class of technologically important oxygen-conducting materials, perovskites may, along with fluorites, also benefit from strain-enhanced transport. For example, in SOFCs, which commonly use perovskite and fluorite materials, the major efficiency losses at low or intermediate temperature occur in the cathode and electrolyte, and can be mitigated by improving the rate of the oxygen reduction reaction at the cathode, and the rate of oxygen transport in both the cathode and the electrolyte.[2] One experimental study of strain effects on oxygen surface exchange and oxygen transport has been carried out on the perovksite Strontium-doped $LaCoO_3$,

with the oxygen tracer diffusion coefficient D* increasing by about 1 order of magnitude when going from a compressive strain to a tensile strain, with a total strain difference of about 2.9%.[10] With some very significant assumptions and approximations, including that the whole increase is due to changes in the migration energy (see Results and Discussion), this increase corresponds to a DMEPS of -64 meV/% strain for out-of-plane hops. Another study on perovskite thin films of $(La_{0.5}Sr_{0.5})CoO_3$ on $SrTiO_3$ argued that changes in oxygen content and ordering were enabled by enhanced cation migration. While this work did not address changes in oxygen migration, it did suggest that the cation migration barriers were significantly enhanced by strain in the sample.[19] Additional studies link tensile strain with enhanced oxygen vacancy formation,[20, 21] which will also contribute to enhanced oxygen diffusion, and potentially to enhanced catalytic activity.[8, 21, 22] The present study aims to survey a range of perovskite materials and develop an understanding of how strain couples to migration barriers, assess the ability to understand these strain effects in terms of a simple elasticity model, and provide guidance on which materials might respond most strongly to strain engineering of oxygen kinetics.

This computational study focuses on bulk conduction and therefore most immediately serves as a foundation to understand strain effects in a system with strain over bulk-like distances, e.g., as may occur in a thin film used in experiments or small devices. However, the bulk trends may also provide guidance for understanding strain effects occurring at interfaces,[11], including surfaces, oxide superstructures,[23] and oxide heterostructures,[24-28] where strain effects may contribute to enhanced performance at perovskite material interfaces.[20, 29]

Using SOFCs as an example, an increase in ionic conductivity of just two orders of magnitude can transform a substandard material into a useful one at intermediate temperatures, so changes on this scale are of significant interest.[2, 30] In terms of specific devices, micro-SOFCs

are on a size scale where epitaxial strain might be used, for example in anode- or cathode-supported electrolyte growth for parallel-layer devices. For a single-chamber configuration,[31, 32], lattice mismatch with the electrolyte may support strained anode or cathode growth.

Motivated by the potential to engineer oxygen conductors with strain and the limited knowledge of strain effects on perovskites, we here study the effects of elastic strain on the oxygen ion conductivity of perovskite systems of the type ABO_3, where A=La and B is a metal ion. Perovksites closely related to this set, with La and other rare earths on the A-site, typically with A-site doping by Sr or other alkali-earth elements and often multiple B site metals, are being used or considered as fast oxygen conductors in SOFCs, oxygen separation membranes and sensors, and chemical looping applications.[1-5] Therefore, the ability to enhance these materials with strain could have significant technological impact.

Results and Discussion

In order to check the coupling between strain and oxygen ion conductivity, we take the migration barrier E_{mig} as a simplified measure of conductivity, as described by Chroneos et al. (see Supporting Information Section S9 for details).[18] We employed the Vienna *Ab-initio* Simulation Package (VASP)[33-36] for density functional theory (DFT) calculations, using the MAterials Simulation Toolkit (MAST)[37] to automate sets of calculation workflows. See the Methods section and Supporting Information for more information on the parameters and workflow used. The Supporting Information also includes detailed discussion on additional hops not shown in the main text, derivation of the parameters used in the elastic strain model, and error analysis.

For the unit cells cells used in these studies, there are multiple symmetry-distinct hops, which increase in number when strain is introduced. In order to keep the calculations tractable, we have studied only a few specific hops for all systems and strain states, and all hops for just a couple of systems. Figure 1 shows the migration barrier versus strain results for a consistent (i.e., the same hopping atom and vacancy sites for each B cation) in-plane hop across all systems. The slope of each line gives the DMEPS value for that system. Figure 2 shows schematically what is meant by an in-plane and out-of plane hop with respect to the strain axes. Positive percent strain is tensile strain and negative percent strain is compressive strain. All systems show a decrease in migration barrier with increasing tensile strain. The average DMEPS is -66 meV per percent strain, with low and high magnitudes for DMEPS of -36 and -89 meV/% strain.

Supporting Information Section S8 shows the following additional details. First, a consistent out-of-plane hop gives comparable DMEPS results to that of the selected in-plane hop across all systems. Second, the selected in-plane and out-of-plane hops are among the lower barrier hops across all systems at zero strain, and are therefore a reasonable representative choice to model diffusion behavior in the perovskites. However, there is no evidence that suggests that the magnitude of a zero-strain migration barrier is correlated with the magnitude of its DMEPS. Therefore, all hops may need to be considered when considering the range of DMEPS for a material. Finally, third, for the cases where we have calculated DMEPS for all hops in the system (a total of 96 hops, of which 12 are symmetry-independent, producing distinct migration barrier values), there is no clear distinction between the magnitudes of DMEPS for in-plane hops versus DMEPS for out-of-plane hops; DMEPS for in-plane hops are neither consistently higher nor consistently lower than those for out-of-plane hops. Therefore, this main text limits the tabulated values to a single consistent hop (in-plane is chosen arbitrarily) and adds an additional range of

+/- 25 meV/% strain to the uncertainty in the calculated DMEPS in order to reflect the range of all the hops possible in a given system. We also note that the effects of strain apply, apparently similarly, to both in-plane and out-of-plane hops.

Table 1 shows the values of the fitted DMEPS from Figure 1, along with their fitting errors. The scatter in some of the DMEPS comes from structural instability (e.g. polymorphs), magnetic instability, and convergence problems, which we discuss in Supporting Information, Section S10, along with our general methodology. Despite the data scatter, we are confident that the trend of decreasing migration barrier with increasing tensile strain (negative DMEPS) is reproducible and significant for the perovskite systems.

Although strain may result in faster interfacial conduction along the plane of the strained interface,[11] our results are for bulk single-crystal conduction and therefore these results represent changes in the properties of bulk strained materials.

Figure 3 compares the DMEPS values obtained in this work with those obtained in other works of which we are aware. Where a log change in diffusion coefficient was given in the literature, the given temperature and lattice mismatch or strain were used to convert the log change in diffusion coefficient into a DMEPS value, making the significant approximation that all changes in diffusion coefficient were due to changes in migration barrier (see the following discussion on Figure 4, as well as Supporting Information, Section S9). The average DMEPS from this study are generally similar to those that have been found previously for both fluorites and perovskites and with both calculations and experiments. While there is no reason that the perovskites should have the quantitatively same DMEPS as the fluorites, it is reasonable to

expect some similarity, given that they are both relatively open-structured oxides, and this qualitative agreement provides some validation of our results.

Figure 4 shows a more quantitative comparison between our DMEPS calculated for $LaCoO_3$, which is -80 meV/% strain for the out-of-plane hop (see Supporting Information, Section S8), and a DMEPS for Sr-doped $LaCoO_3$ (LSC) perovskite derived from Kubicek et al.'s experimental LSC oxygen diffusion data along the out-of-plane direction,[10] which we estimate as -64 meV/% strain. This comparison is the closest comparison that can be made between our calculated systems and those studied experimentally to this point. Note that we derive the DMEPS from the experimental data of the LSC under the assumption that all changes are due to only changes in migration barrier (see Supporting Information, Section S9). This assumption is certainly an approximation given that an increase in Co reduction is observed in strained LSC in experiment,[38] and that the oxygen vacancy formation energy in undoped $LaCoO_3$ was calculated to decrease with tensile strain within 2% tensile strain,[39] both of which may indicate increased oxygen vacancy concentration with strain. Neglecting this vacancy increase may lead to an overestimation in our DMEPS derivation. We also note that no reduction in activation energies was measured by Kubicek, et al., although there was significant uncertainty in the measurements.[10] In addition, while we took the experimental 475°C strain range of -1.9% compressive to 1.0% tensile strain for our derivation,[10] any strain relaxation that occurred in the film may also modify the derived DMEPS. Despite these limitations on the comparison, it is encouraging that the DMEPS for our out-of-plane hop, and also the DMEPS for our in-plane hop, at -60 meV/% strain, are both in good agreement with the DMEPS estimated from experiment. The good agreement provides some support for the results of our calculations and supports the hypothesis that at least some of the oxygen transport changes seen in the

experimental studies of Kubicek, et al. are in fact due to bulk changes in migration energies induced by strain.

Overall, our total range of DMEPS represent values significantly lower and higher than previously reported, which is likely due to the relatively large number of compounds we have studied. Our results demonstrate that, even within one crystal structure, changing B-site cations can lead to a very wide range of oxygen migration strain response.

To explain the observed decrease of migration barrier with increasing percent biaxial strain, we consider the elastic model of Schichtel et al.,[12] which is given as Equation 1. First we convert this equation into a form where we can compare the predicted DMEPS value from this equation to that obtained from our calculations. Equation1 uses the Young's modulus Y, Poisson's ratio v, and applied biaxial strain ϵ_{12} to calculate a pressure p due to strain. We take this pressure p to be equivalent to a change in pressure Δp compared to an assumed zero pressure at zero strain ($\Delta p = p - 0$). Dividing both sides by ϵ_{12} gives a slope of change in pressure with percent strain. Multiplying both sides by migration volume V_{mig} transforms the slope of change in pressure with percent strain into a slope of change in migration free energy G_{mig} per percent strain, which we then approximate by the change in migration enthalpy H_{mig} per percent strain, as shown in Equation 2. Details of these derivations and calculations are in the Supporting Information, Section S12). For each strain case, our constant-volume migration barrier energies E_{mig} are directly comparable to constant-pressure migration enthalpies (see Supporting Information, Section S9a), and therefore we also use DMEPS as the term for the elastic model slope of change in migration enthalpy per percent strain. Now the DMEPS predicted from Schichtel et al.'s elastic model and our ab initio calculation can be compared directly.

$p = -\frac{2}{3}\left(\frac{Y}{1-\nu}\right)\epsilon_{12}$	Eq. 1
$\frac{\Delta p * V_{mig}}{\epsilon_{12}} = -\frac{2}{3}\left(\frac{Y}{1-\nu}\right)V_{mig} = \frac{\Delta G_{mig}}{\epsilon_{12}} \approx \frac{\Delta H_{mig}}{\epsilon_{12}}$	Eq. 2

Figure 5 shows the elastic model DMEPS in meV/% strain as a function of the DMEPS we calculated directly from ab-initio DFT methods. From this figure, we see that the DMEPS predicted by the strain model qualitatively follow the same trends as our ab-initio DMEPS. The strain model DMEPS differ from the DFT-calculated DMEPS by an average of 16 +/- 13 meV/% strain (where the uncertainty represents one standard deviation of the error from the mean), with a maximum error of 40 meV/% strain and a root-mean-squared error of 20 meV/% strain, over all in-plane and out-of-plane hops shown in Figure 5. An equivalent but distinct approach to assessing the strain model is to use the ab-initio calculated DMEPS and the strain model to estimate vacancy migration volume and then compare this volume to the directly ab-initio calculated vacancy migration volume (see Supporting Information, Section S12d). This perspective shows that the effective migration volumes predicted by the strain model are similar to those calculated directly using the ab-initio methods, with some outliers. The root-mean-squared error for predicting migration volumes is 2 $Å^3$. The source(s) of discrepancies between the strain model results and the ab-initio data are not clear at this stage. The error is not as simple as a strain-dependent migration volume, as that would lead to a strong non-linear dependence in the ab-initio calculated DMEPS, whose constituent points are generally fairly linear. It might also be proposed that the presence of the vacancies alters the elastic properties, as has been predicted in some cases [19], as all the elastic constants are determined for the pristine

material with no vacancies. Checks with select systems have shown that using elastic properties in the presence of vacancies can shift the predicted elastic-model DMEPS by some -10 to -20 meV/% strain, which in some cases may lead to better agreement, but still leaves significant deviation between the model and the fit results (see Supporting Information, Section S12b). We hypothesize that anisotropic effects account for the main deviations from the strain model, as the strain model uses a single isotropic pressure value and a single isotropic migration volume value. Other effects could include anharmonic effects causing deviations from linear elasticity and numerical noise in the calculations, particularly regarding the migration volumes.

Additional analysis, January 2016:

> Since the elastic strain model uses the zero-strain migration volume, its representation of the DFT DMEPS is expected to be most accurate near zero strain and less accurate for larger strains. Table E1 shows all slopes refit using only data between -1% and 1% strain. Figure E1 shows the agreement between the elastic strain model DMEPS and the low-strain DFT DMEPS. Comparing Figure E1 and Figure 5R shows a small improvement when using the low-strain data, resulting in an average difference of 14 +/- 12 meV/% strain with a maximum difference of 47 meV/% strain and a root-mean-squared error of 18 meV/% strain.
>
> The $LaCrO_3$ system may best describe the limit of the present elastic strain model's accuracy for representing DFT-fit DMEPS. Its well-behaved elastic constant fits lead to small error bars in the elastic model DMEPS (Table S12.2R). Its DFT migration barrier data, which follows a smooth and consistent slope along the -2% to 2% range of strain, leads to small error bars in the DFT DMEPS, whether the DFT DMEPS is calculated between -2% and 2% strain or between -1% and 1% strain (Figure 1, Figure S8.1R). Nevertheless, both the in-plane hop and the out-of-plane hop in Figure 5R show a disagreement between the elastic model DMEPS and the DFT DMEPS of approximately 20 meV/% strain. The range of disagreement is approximately 30 meV/% strain when all hops are considered (Figure S8.9R).
>
> Using a defected bulk modulus to calculate Young's modulus for the prefactor does not reduce the disagreement between the elastic model DMEPS and the DFT-fit DMEPS for both the in-plane hop and the out-of-plane hop in $LaCrO_3$ (see Figure S12.2R). Using a volume-relaxed migration volume rather than the Birch-Murnaghan fit migration volume also does not reduce the disagreement for both points (see Figure S12.5R).

Having examined each variable in the elastic model, we conclude that while the elastic model DMEPS are in qualitative agreement with the DFT-fit DMEPS, the error in the best fit cases is still approximately 30 meV/% strain for a single system considering all hops, approximately 20 meV/% strain for a single hop, and is more accurate at low strains for systems where the strain response is non-linear over a larger strain range.

Future modifications to the elastic model to yield better accuracy might include the use of anisotropic migration volumes and full elastic constant tensors. However, the inclusion of so much calculated data to the elastic model may disrupt the simplicity and generality of the approach. We reiterate that on the whole, the isotropic elastic model appears to qualitatively describe the response of oxygen migration barriers in perovskites with respect to biaxial strain.

Methods

To calculate E_{mig}, we used density functional theory (DFT) as implemented in the Vienna Ab-initio Simulation Package (VASP)[33] with the climbing nudged elastic band method (CNEB) with 3 images.[40, 41] The pseudopotentials used were generated using the generalized gradient approximation and the projector-augmented-wave method[42, 43] with the Perdew-Wang 91 exchange correlation functional.[44-46] Valence electrons are listed in parentheses. The standard La pseudopotential was used ($5s^2 5p^6 5d^1 6s^2$). For the transition metals, the available pseudopotential with the most unfrozen electrons was used to assure the best possible accuracy: Sc_sv ($3s^2 3p^6 3d^1 4s^2$), Ti_sv ($3s^2 3p^6 3d^2 4s^2$), V_sv ($3s^2 3p^6 3d^3 4s^2$), Cr_pv ($3p^6 3d^4 4s^2$), Mn_pv ($3p^6 3d^5 4s^2$), Fe_sv ($3s^2 3p^6 3d^6 4s^2$), Co ($3d^7 4s^2$), Ni_pv ($3p^6 3d^8 4s^2$), and Ga_d ($3d^{10} 4s^2 4p^1$). The soft oxygen pseudopotential was used.

A starting supercell of 2x2x2 formula units (40 atoms) was used, with 4x4x4 kpoints in a Monkhorst-Pack scheme.[47] Migration barriers were converged to within 20 meV relative to the choice of kpoint mesh. All calculations are started with the B-site cations in a ferromagnetic configuration. The same two migration directions were calculated for each system; one with an oxygen atom traveling within the plane of the strain, and one with an oxygen atom traveling out of the plane of the strain. Systems were strained equally along lattice parameters *a* and *b* by at

least a grid of 0, ±1%, and ±2% of the original lattice parameters, with positive percentages as tensile strain and negative percentages as compressive strain, and a fit was performed in each strain case to find the equilibrium lattice parameter perpendicular to the plane (*c* lattice parameter). All CNEB calculations were performed at constant volume with internal relaxation. Calculation workflows were automated using the MAterials Simulation Toolkit (MAST), which is under development at the University of Wisconsin-Madison.[37]

We create a vacancy by removing from the supercell both an oxygen atom with its six electrons and an additional two electrons (see a discussion in Supporting Information, Section S7). This procedure is the computational equivalent of substituting lower-valence dopant atoms on A-sites or B-sites somewhere else in the crystal beyond the boundaries of the supercell. The advantage of this method is that it avoids the interaction between oppositely-charged defects by creating a single oxygen vacancy in the supercell without using dopant atoms.

For details on cutoff energy, smearing, CNEB parameters, CNEB workflow, simplifications involved, strain parameters, and charge compensation methods, see Supporting Information.

Conclusions

We calculate that epitaxial tensile strain can reduce the migration barrier in perovskites with an overall average of about -65 meV per percent strain, with low and high DMEPS magnitudes of -36 and -86 meV/% strain, for a consistent in-plane hop. Assuming no other factors play a role, this decrease in barrier implies an overall average increase in ionic

conductivity of about 2.5 orders of magnitude for a 2% biaxial tensile strain at 300K for some of the most responsive materials calculated here ($LaCrO_3$).

The amount of change depends strongly on the individual material and its DMEPS. On average, a 2% strain is not enough to transform a poor ionic conductor into a good ionic conductor, e.g. the strain effect on migration barrier is not enough to transform $LaTiO_3$ and $LaVO_3$ with high calculated migration barriers into the same class of high-performing oxygen conductors as La[Mn, Fe, Sc, Ga]O_3 with their lower migration barriers. However, the effect may be enough to extend the temperature range of a good high-temperature ionic conductor into a significantly lower temperature region. For example, the ionic conductivity of ionic conductors yttria-stabilized zirconia (YSZ), yttria-stabilized bismuth oxide (YSB), and $LaGaO_3$ with Sr, Mg, and Co doping (LSGMC) decline by about 2.4, 0.7, and 0.9 orders of magnitude between 750°C and 500°C,[2] which take them out of the usable range for SOFCs by 500°C; a single order of magnitude change could potentially be recouped using strain, and allow these materials to be used at 500°C. However, we note that maintaining significant strains in bulk materials over long times and at high-temperature, as occur in SOFCs, is extremely challenging. Therefore, the most likely role for strain to enhance SOFC systems is in thin-film devices or at interfaces. Overall, the strain effect on migration barrier in the perovskites studied here suggests that strain should be considered as a method for producing or enhancing perovskite fast oxygen-ion conductors for applications such as low or intermediate temperature SOFCs, gas separation membranes, chemical looping devices, and memristors.

The origin of the strain effects on migration energy is still somewhat unclear. We find that the effects of strain on migration barrier can be captured qualitatively by a simple migration volume elasticity model. The error in the elastic model DMEPS predictions using an ab-initio

calculated migration volume is 16 +/- 13 meV/% strain compared to the DMEPS fit to DFT-calculated data.

Additional aspects of the migrating oxygen beyond its migration volume, perhaps associated with local distortions during migration, appear to be playing a significant role in the strain response of anion migration in these perovskite systems.

Another interesting challenge raised by this work is to understand the origin of the variability of strain response across different B cations, which we here demonstrate to range in DMEPS by over 50 meV/% strain across the B-site cations for a consistent hop. Our efforts at correlations with B-site cation size, d-electron filling, and other plausible descriptors did not yield any robust correlations. Understanding the origin of this variability in terms of controllable parameters could yield novel materials that are engineered to respond most effectively to strain.

Acknowledgments

We would like to acknowledge the NSF Graduate Fellowship Program under Grant No. DGE-0718123 for partial funding of T. Mayeshiba. We would also like to thank the Professor Emeritus Raymond G. and Anne W. Herb Endowment for Physics, the UW-Madison Graduate Engineering Research Scholars Program, and the Robert E. Cech materials science scholarship for additional support of T. Mayeshiba. Computing resources in this work benefitted from the use of the Extreme Science and Engineering Discovery Environment (XSEDE), which is supported by National Science Foundation grant number OCI-1053575, and from the computing resources and assistance of the UW-Madison Center For High Throughput Computing (CHTC) in the Department of Computer Sciences. The CHTC is supported by UW-Madison and the Wisconsin Alumni Research Foundation, and is an active member of the Open Science Grid, which is supported by the National Science Foundation and the U.S. Department of Energy's

Office of Science. Support for D. Morgan, conference travel funds for D. Morgan and T. Mayeshiba, and the MAST tools applied in this work were provided by the NSF Software Infrastructure for Sustained Innovation (SI^2) award No. 1148011. We thank M. Gadre for helpful discussions about stress and strain.

Supporting Information

Supporting information is available and describes the following:

S1. Strain notation

S2. The 2x2x2 supercell and atomic positions

S3. Our orthorhombic-to-cubic assumption

S4. Pseudopotentials, electron smearing, and climbing nudged-elastic band calculations

S5. GGA versus GGA+U

S6. Ferromagnetic, high-spin starting configuration

S7. Charge compensation

S8. Jump directions, including all barriers for B=Mn and B=Cr

S9. Migration energy and its relationship to ionic conductivity

S9a. Relating H_{mig} at Constant Pressure and E_{mig} at Constant Volume, for Unstrained and Strained Cases

S9b. Approximating the Defected Volume with the Undefected Volume

S10. Straining supercells and the strained workflow

S11. Fitting and error analysis

S12. The elastic strain model

S12a. Finding Poisson's ratio

S12b. Finding bulk modulus

S12c. Finding Young's modulus

S12d. Finding migration volume

Figures and Tables

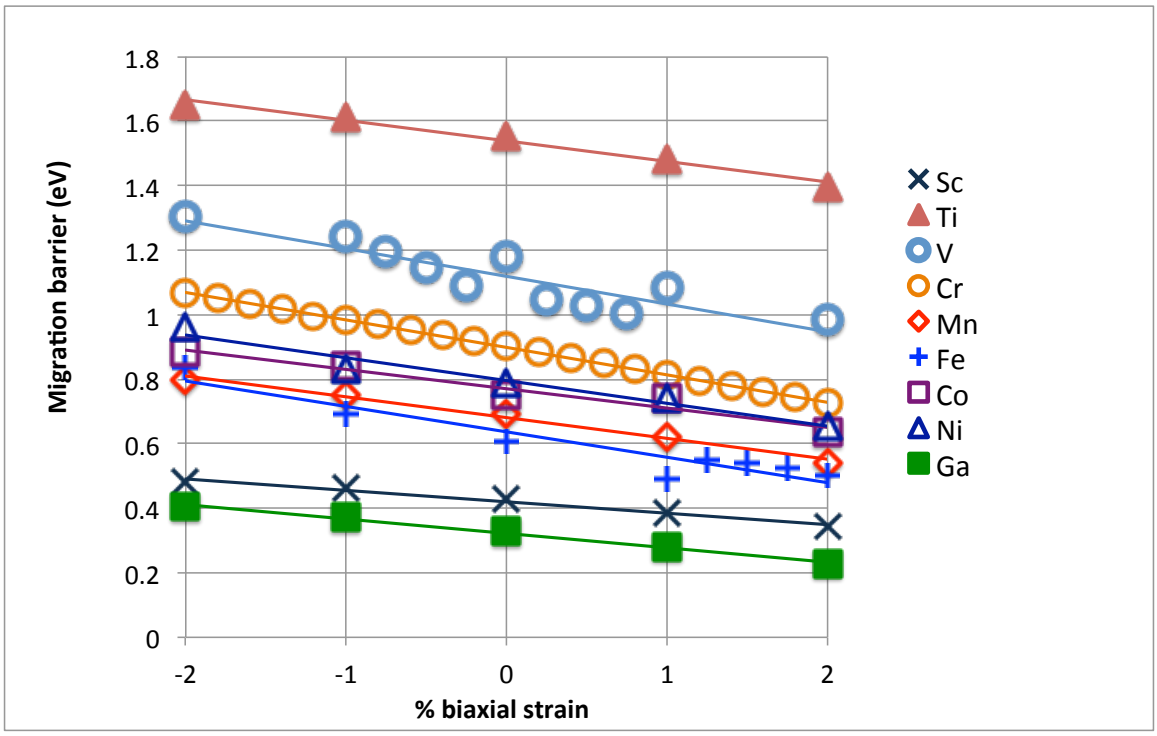

Figure 1. Migration barrier versus strain for a selected in-plane hop, which is shown schematically in Figure 2. See ESI, Section S2, for the atomic positions used (o31 to o30). The slope of each line is referred to in-text as a "DMEPS" value, which stands for "Delta (change) in Migration Energy per Percent Strain."

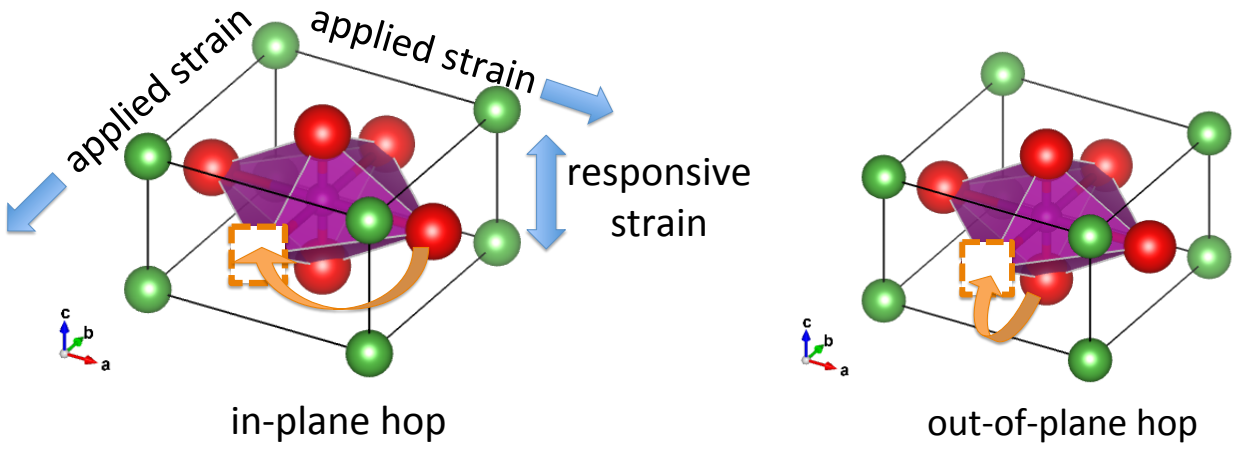

Figure 2. Schematic of an in-plane hop (left) and an out-of-plane hop (right) relative to the strain axes. The A-site cation is in green ("box corners"), the B-site cation is in purple (octahedral center), and the oxygen atoms are in red (octahedral vertices). The oxygen vacancy position is shown as an empty box with a dashed outline. This schematic shows an exaggerated example of applied biaxial tensile strain and its accompanying responsive compressive strain. For simplicity,

only a 1x1x1 segment of the actual 2x2x2 supercell is shown, and octahedral tilting is not depicted. See Supporting Information Section S2 for more detailed supercell information.

Table 1. DFT-fit DMEPS values and their errors. See ESI, Section S11, for error calculations. All numbers are in meV/% strain. While the total error range may suggest the possibility of positive DMEPS, we expect that the error estimates are not accurate in this region as we find no evidence for positive DMEPS and do not expect them for any similar perovskite systems.

B-site cation	DMEPS fit to DFT (meV/% strain)	DMEPS fitting error (+/- meV/% strain)	Estimated bound for DMEPS over all hops (+/- meV/% strain)
Sc	-36	3	28
Ti	-64	5	30
V	-86	14	39
Cr	-85	0.4	25
Mn	-64	4	29
Fe	-79	10	35
Co	-60	8	33
Ni	-70	8	33
Ga	-44	2	27

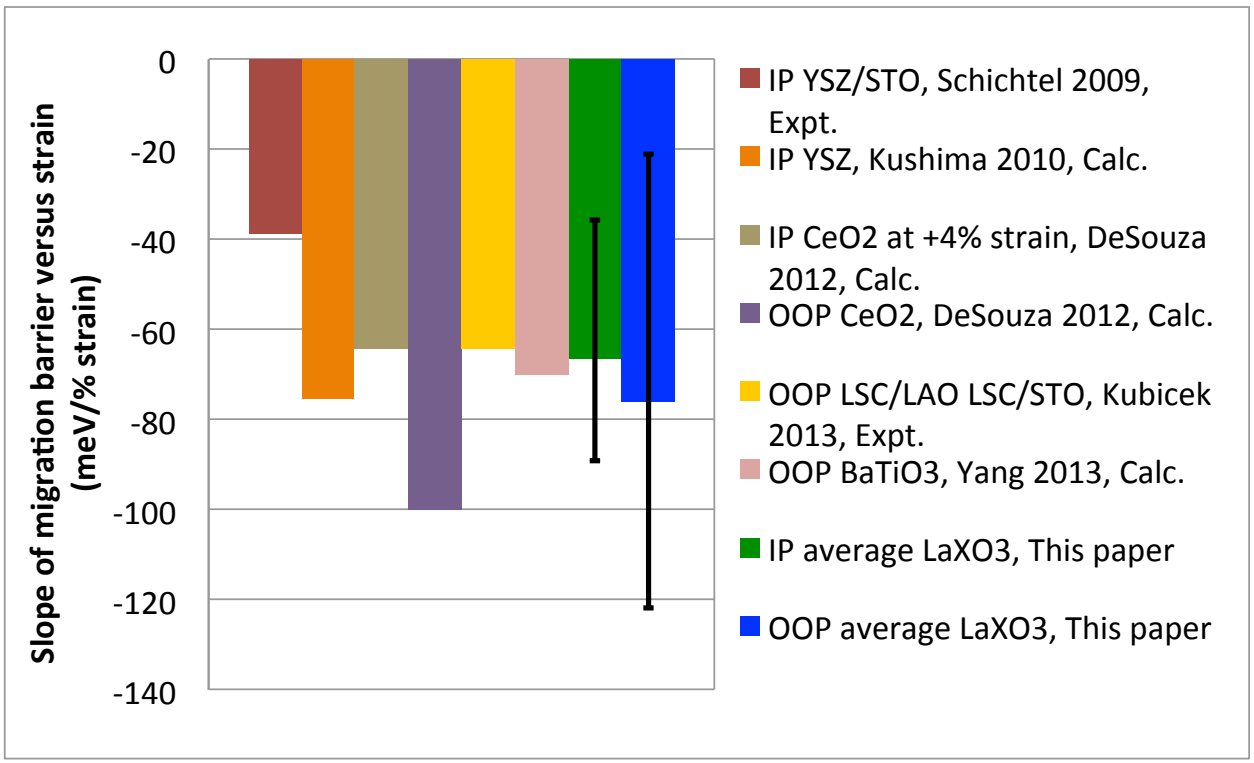

Figure 3. Comparison of literature values[3, 10, 12, 15] with values from this study. Error bars on the values from this study indicate the largest and smallest in-plane (IP) and out-of-plane (OOP) DMEPS values that were calculated for any system. DMEPS stands for "Delta (change) in Migration Energy per Percent Strain".

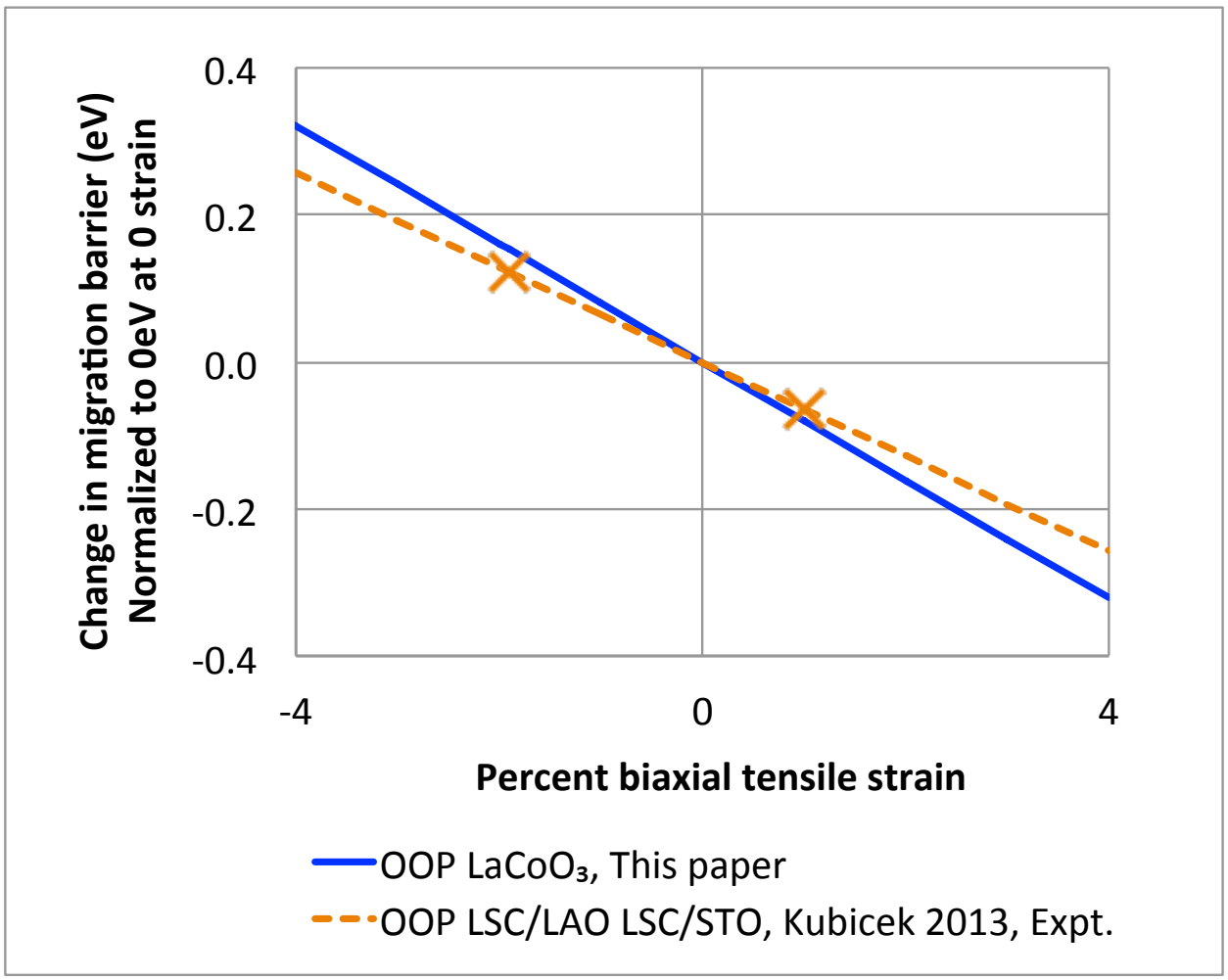

Figure 4. Comparison between our $LaCoO_3$ DMEPS for bulk oxygen diffusion and the Sr-doped LaCoO3 DMEPS for oxygen surface-to-depth diffusion of Kubicek et al.[10] DMEPS stands for "Delta (change) in Migration Energy per Percent Strain".

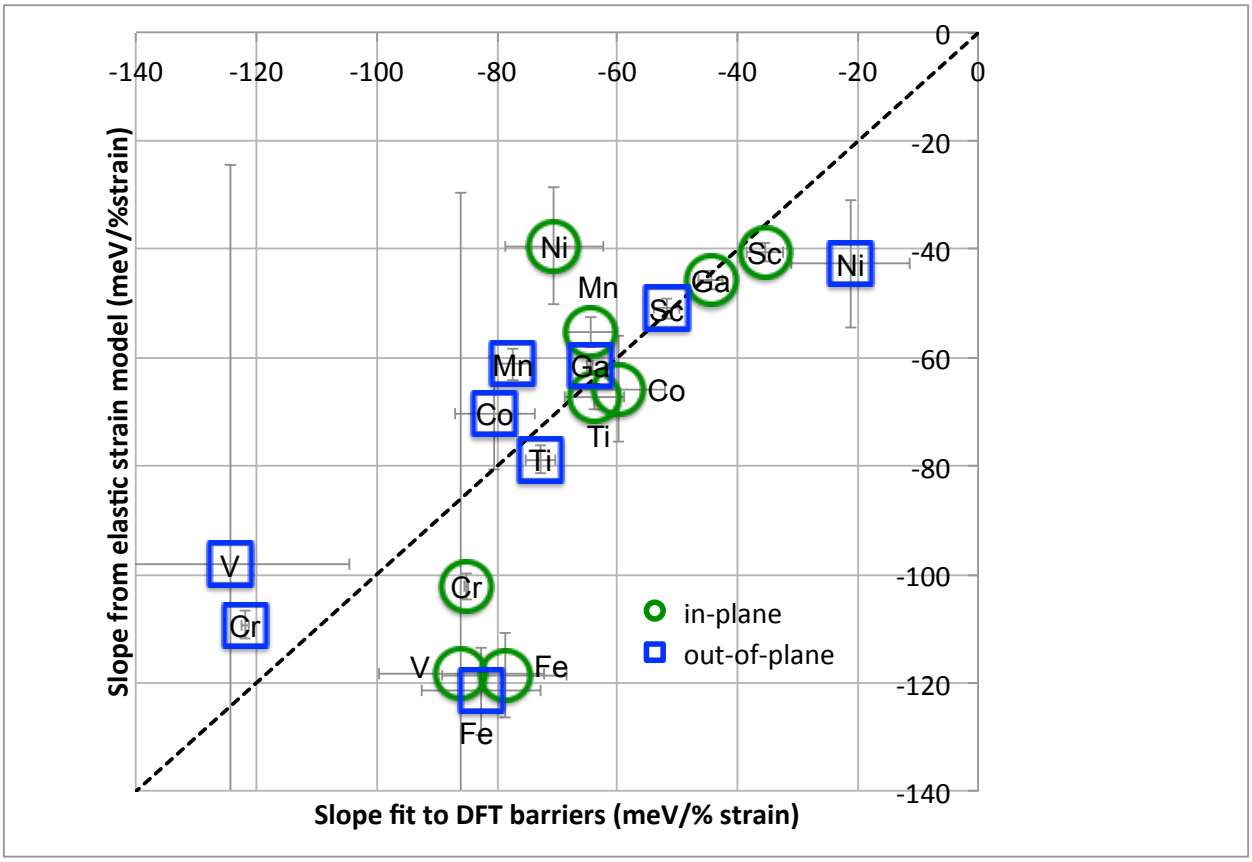

Figure 5. Elastic formula DMEPS versus fitted DMEPS for migration barrier as a function of strain (dashed line indicates perfect match). Data point is the center of each symbol. Error bars are based on uncertainties in fitting elastic constants and are discussed in the Supporting Information, Section S12. DMEPS stands for "Delta (change) in Migration Energy per Percent Strain". All error bars are symmetric.

Table E1. DFT-fit DMEPS using only biaxial strains between -1% and 1%.

B-site	In-plane DMEPS fit to DFT (meV/% strain)	In-plane DMEPS fitting error (+/- meV/% strain)	Out-of-plane DMEPS fit to DFT (meV/% strain)	Out-of-plane DMEPS fitting error (+/- meV/% strain)
Sc	-37	2	-54	0.4
Ti	-65	4	-75	1
V	-99	26	-131	39
Cr	-86	1	-124	1
Mn	-65	4	-72	3
Fe	-99	8	-113	6
Co	-51	23	-100	11
Ni	-47	2	4	0.5
Ga	-45	2	-65	0.5

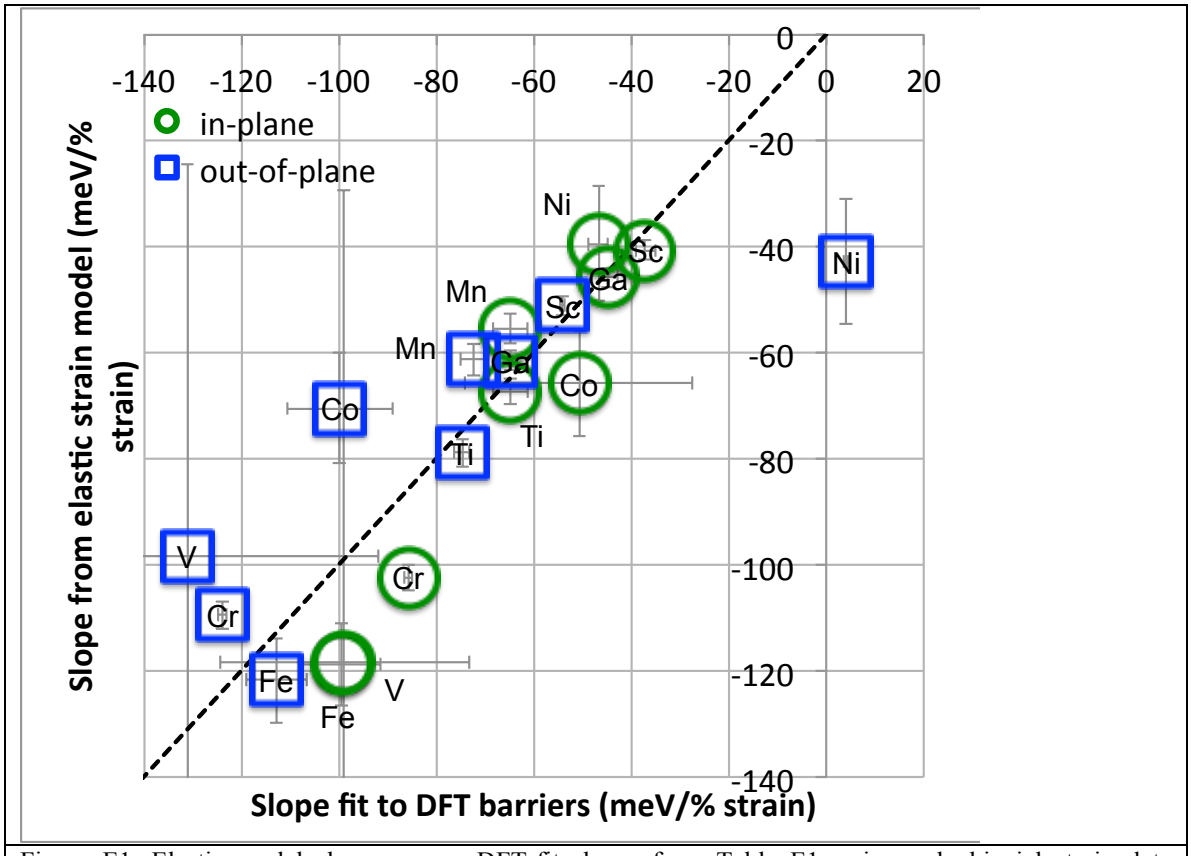

Figure E1. Elastic model slopes versus DFT-fit slopes from Table E1, using only biaxial strain data between -1% and 1%. The B-site cation Nickel point has a positive DFT-fit slope between -1% and 1%, producing the outlying position shown here, but its overall slope with strain is actually negative (see Figure S8.1R). The points for in-plane B-site cations Iron and Vanadium occupy a nearly identical spot.

References

1. M. Arjmand, A. Hedayati, A.-M. Azad, H. Leion, M. Rydén and T. Mattisson, *Energy & Fuels*, 2013, 27, 4097-4107.
2. D. J. L. Brett, A. Atkinson, N. P. Brandon and S. J. Skinner, *Chemical Society Reviews*, 2008, 37, 1568-1578.
3. R. A. De Souza and J. A. Kilner, *Solid State Ionics*, 1998, 106, 175-187.
4. F. He, K. Zhao, Z. Huang, X. a. Li, G. Wei and H. Li, *Chinese Journal of Catalysis*, 2013, 34, 1242-1249.
5. P. Knauth and H. L. Tuller, *J Am Ceram Soc*, 2002, 85, 1654-1680.
6. S. Schweiger, M. Kubicek, F. Messerschmitt, C. Murer and J. L. M. Rupp, *ACS nano*, 2014, 8, 5032-5048.
7. S. Kim, S. Choi and W. Lu, *ACS Nano*, 2014, 8, 2369-2376.
8. B. Yildiz, *MRS Bulletin*, 2014, 39, 147-156.
9. J. Garcia-Barriocanal, A. Rivera-Calzada, M. Varela, Z. Sefrioui, E. Iborra, C. Leon, S. J. Pennycook and J. Santamaria, *Science*, 2008, 321, 676-680.
10. M. Kubicek, Z. Cai, W. Ma, B. Yildiz, H. Hutter and J. Fleig, *ACS nano*, 2013, 7, 3276-3286.
11. C. Leon, J. Santamaria and B. A. Boukamp, *MRS Bulletin*, 2013, 38, 1056-1063.
12. N. Schichtel, C. Korte, D. Hesse and J. Janek, *Physical chemistry chemical physics : PCCP*, 2009, 11, 3043-3048.
13. M. Sillassen, P. Eklund, N. Pryds, E. Johnson, U. Helmersson and J. Bottiger, *Advanced Functional Materials*, 2010, 20, 3194-3194.
14. R. A. De Souza, A. Ramadan and S. Hörner, *Energy & Environmental Science*, 2012, 5, 5445.
15. A. Kushima and B. Yildiz, *Journal of Materials Chemistry*, 2010, 20, 4809.
16. Q. Yang, J. X. Cao, Y. Ma, Y. C. Zhou, L. M. Jiang and X. L. Zhong, *Journal of Applied Physics*, 2013, 113.
17. M. Mogensen, D. Lybye, N. Bonanos, P. V. Hendriksen and F. W. Poulsen, *The effect of lattice stress in ion conducting fluorites and perovskites*, Electrochemical Society Inc, Pennington, 2002.
18. A. Chroneos, B. Yildiz, A. Tarancón, D. Parfitt and J. A. Kilner, *Energy & Environmental Science*, 2011, 4, 2774.
19. W. Donner, C. L. Chen, M. Liu, A. J. Jacobson, Y. L. Lee, M. Gadre and D. Morgan, *Chem Mater*, 2011, 23, 984-988.
20. H. Jalili, J. W. Han, Y. Kuru, Z. H. Cai and B. Yildiz, *Journal of Physical Chemistry Letters*, 2011, 2, 801-807.
21. A. Kushima, S. Yip and B. Yildiz, *Physical Review B*, 2010, 82.
22. J. Wintterlin, T. Zambelli, J. Trost, J. Greeley and M. Mavrikakis, *Angewandte Chemie International Edition*, 2003, 42, 2850-2853.
23. R. Sayers, F. Schiffmann, S. Fearn, J. A. Kilner, B. Slater, S. Romani, D. J. Tatham, J. B. Claridge, F. Cora and M. J. Rosseinsky, *Chem Mater*, 2013, 25, 3441-3457.
24. Z. Feng, Y. Yacoby, M. J. Gadre, Y.-L. Lee, W. T. Hong, H. Zhou, M. D. Biegalski, H. M. Christen, S. B. Adler, D. Morgan and Y. Shao-Horn, *The Journal of Physical Chemistry Letters*, 2014, 5, 1027-1034.
25. M. Sase, *Solid State Ionics*, 2008, 178, 1843-1852.

26. D. Lee, A. Grimaud, E. J. Crumlin, K. Mezghani, M. A. Habib, Z. X. Feng, W. T. Hong, M. D. Biegalski, H. M. Christen and Y. Shao-Horn, *Journal of Physical Chemistry C*, 2013, 117, 18789-18795.
27. M. J. Gadre, Y. L. Lee and D. Morgan, *Physical Chemistry Chemical Physics*, 2012, 14, 2606-2616.
28. Y. Chen, Z. H. Cai, Y. Kuru, W. Ma, H. L. Tuller and B. Yildiz, *Advanced Energy Materials*, 2013, 3, 1221-1229.
29. J. W. Han and B. Yildiz, *Energy & Environmental Science*, 2012, 5, 8598-8607.
30. E. D. Wachsman and K. T. Lee, *Science*, 2011, 334, 935-939.
31. H. Kim, S.-H. Choi, J. Kim, H.-W. Lee, H. Song and J.-H. Lee, *Journal of Materials Processing Technology*, 2010, 210, 1243-1248.
32. J. P. Viricelle, S. Udroiu, G. Gadacz, M. Pijolat and C. Pijolat, *Fuel Cells*, 2010, 10, 683-692.
33. G. Kresse and J. Furthmuller, *Physical Review B*, 1996, 54, 11169-11186.
34. G. Kresse and J. Furthmüller, *Computational Materials Science*, 1996, 6, 15-50.
35. G. Kresse and J. Hafner, *Physical Review B*, 1993, 47, 558-561.
36. G. Kresse and J. Hafner, *Physical Review B*, 1994, 49, 14251-14269.
37. T. Angsten, T. Mayeshiba, H. Wu and D. Morgan, *New Journal of Physics*, 2014, 16, 015018.
38. Z. Cai, Y. Kuru, J. W. Han, Y. Chen and B. Yildiz, *J Am Chem Soc*, 2011, 133, 17696-17704.
39. A. Kushima, S. Yip and B. Yildiz, *Physical Review B*, 2010, 82, 115435.
40. G. Henkelman, B. P. Uberuaga and H. Jónsson, *The Journal of Chemical Physics*, 2000, 113, 9901.
41. D. Sheppard, R. Terrell and G. Henkelman, *J Chem Phys*, 2008, 128, 134106.
42. P. E. Blochl, *Physical review. B, Condensed matter*, 1994, 50, 17953-17979.
43. G. Kresse and D. Joubert, *Physical Review B*, 1999, 59, 1758-1775.
44. J. P. Perdew, K. Burke and M. Ernzerhof, *Phys Rev Lett*, 1996, 77, 3865-3868.
45. J. P. Perdew, K. A. Jackson, M. R. Pederson, D. J. Singh and C. Fiolhais, *Physical Review B*, 1992, 46, 6671-6687.
46. J. Perdew, K. Burke and M. Ernzerhof, *Phys Rev Lett*, 1996, 77, 3865-3868.
47. H. J. Monkhorst and J. D. Pack, *Physical Review B*, 1976, 13, 5188-5192.